INSTITUTE OF PHYSICS PUBLISHING PHYSICS IN MEDICINE AND BIOLOGY

Phys. Med. Biol. **50** (2005) 2859–2869 doi:10.1088/0031-9155/50/12/009

The influence of measurement uncertainties on the evaluation of the distribution volume ratio and binding potential in rat studies on a microPET® R4: a phantom study

Vesna Sossi[1], Marie-Laure Camborde[2], Giorgia Tropini[1], Danny Newport[3], Arman Rahmim[1], Doris J Doudet[4] and Thomas J Ruth[5]

[1] Department of Physics and Astronomy, University of British Columbia, 6224 Agricultural Rd, Vancouver V6T 1Z1, Canada
[2] University of British Columbia/TRIUMF, 4004 Wesbrook Mall, Vancouver V6T 2A3, Canada
[3] CTI Concorde Microsystems, LLC 10427 Cogdill Rd, Suite 500, Knoxville, TN 37932, USA
[4] Department of Medicine, University of British Columbia, 2221 Wesbrook Mall, Vancouver V6T 2B5, Canada
[5] TRIUMF, 4004 Wesbrook Mall, Vancouver 2A3, Canada

E-mail: vesna@physics.ubc.ca

Received 20 November 2004, in final form 30 March 2005
Published 1 June 2005
Online at stacks.iop.org/PMB/50/2859

Abstract

In small animal positron emission tomography (PET) imaging, the injectable radiotracer dose is often limited by the tracer mass which, together with the tracer kinetics and scanner sensitivity, dictates the statistical quality of the time activity curves (TACs) used to extract biological parameters. We investigated the effect of measurement uncertainty on the determination of the distribution volume ratio (DVR) and binding potential (BP) as estimated using the tissue input Logan (DVR_L, BP_L) and the ratio (DVR_r, BP_r) methods for two tracers, with the Concorde microPET® R4 camera. Parameters' coefficients of variation (COV) were estimated from a combination of rat and phantom data. For ^{11}C-dihydrotetrabenazine, the COV was 11% for the BP_L and 13.4% for the BP_r when using TACs obtained from individual regions of interest (ROIs) and segmented attenuation correction. The COVs were reduced to 7.5% (BP_L) and 8.6% (BP_r) when the striatal and cerebellar TACs were estimated as averages of 3 and 2 ROIs respectively. Results obtained for ^{11}C-methylphenidate (MP) yielded approximately 30% higher COVs. With measured attenuation correction, the COVs were on average 100% higher. The presented method can be used to examine the contribution of a variety of imaging conditions to the uncertainty of biologically meaningful parameters.

Introduction

The advances in the imaging capability of positron emission tomography (PET) instrumentation as well as radiotracer development occurring over the last several years have led to increasingly more complicated imaging protocols aimed at investigating increasingly more complex biological questions. Imaging protocols requiring repeated scans on the same subject under different conditions, such as at baseline and following a specific intervention, are now more frequently performed and often analysed on a one-subject basis. As animal models for various diseases are becoming more and more refined there is increasing interest in investigating detailed disease mechanism using small animals. It is thus very important in this context to determine the accuracy limitations due to the statistical and instrumentation-related quality of the data so as to evaluate the feasibility of the desired investigation. Such analysis is particularly important in small animal receptor imaging where the allowed administered dose is often dictated by biological constraints.

The radiotracer dose in PET neuroreceptor imaging is limited by the requirement that the tracer amount should not occupy more than 1% of the available receptors (Hume *et al* 1998). This requirement is particularly significant in small animal studies: due to their minute size, the maximum amount of radiotracer that can be administered without inducing significant receptor occupancy results in count rates that are generally well below the count rate capabilities of PET cameras. Likewise, the acquisition time for each time frame is generally limited by the need of capturing the changes of the radiotracer distribution as a function of time in sufficient detail to permit an accurate biologically relevant analysis. These two requirements cause the number of acquired counts for each time frame to be often quite low, thus raising the question about the influence of the statistical quality of the acquired data on the variability of the final biological parameter.

Inaccurate quantification corrections are additional possible sources of uncertainty, since they lead to artificial image non-uniformities. This source of uncertainty is not necessarily limited to small animal imaging, but its importance is specific to each camera and each algorithm used for data quantification. For example, for the specific PET scanner used in this study, the CTI-Concorde microPET® R4, attenuation correction factors derived directly from a transmission scan (measured attenuation correction) have been identified as a definite contributor to uniformity degradation (Camborde *et al* 2004). In this study, we have evaluated the contribution of the combined effect of instrumental and statistical source of variability to the uncertainty of two final parameters of interest in neuroreceptor studies, the distribution volume ratio (DVR) and the binding potential (BP). It must, however, be noted that such determination provides only a lower limit to the accuracy of the parameter evaluation, since *in vivo* measurement reproducibility is also influenced by biological variability, which is not addressed in this study.

There are often several methods that can be used to provide estimates of the DVR and BP, each providing a different compromise between biological accuracy and ease of determination. For example, an estimate of the BP, which is the most commonly used parameter to quantify binding of reversible tracers, can be obtained using compartmental models (Lammertsma and Hume 1996, Lammertsma *et al* 1996, Gunn *et al* 1997), simple ratio estimates (Ito *et al* 1998) or graphical methods (Logan *et al* 1990, 1996). Each of these methods may use a different combination of the acquired data: for example, ratio methods often use tracer distribution values averaged over relatively long times (of the order of 30 min), compartmental models use data acquired within each time frame, while graphical methods typically use a combination of time-averaged (or time-integrated) data and values from single time frames. Each of these methods is thus differently sensitive to the statistical noise of the data. In our evaluation, we

considered two methods used to obtain estimates of the BP: the tissue input Logan graphical approach (BP_L) (Logan *et al* 1996), and the simple target to reference region ratio (BP_r), where a ratio between the striatal and cerebellar activity, each averaged over the 30–60 min post-injection, is calculated. In all these methods the directly determined variable is the tracer distribution volume ratio (DVR_L, DVR_r), which is generally related to the BP as DVR = BP+1. Only bloodless methods were considered, since in small animal scanning blood sampling is not easily feasible.

In order to achieve an evaluation of the impact of the statistical and instrumentation-related quality of the data on the final parameter determination, it is necessary to create reproducible image replicas, which may differ only because of the statistical variation of the radioactivity concentration measurement and because of systematic inaccuracies introduced by the imaging procedure. To obtain these conditions, we have created replicas of time activity curves (TACs) representative of those obtained in typical rat ^{11}C-dyhidrotetrabenazine (DTBZ—a monoamine vesicular transporter VMAT2 marker) and ^{11}C-methylphenidate (MP—a dopamine membrane transporter DAT marker) studies by extracting appropriate time frames from a dynamic study of a phantom filled with a uniform radioactivity concentration ('rat phantom'). By placing several identical ROIs on the 'rat-phantom' and evaluating the appropriate radioactivity time distributions, several realizations of the TACs were obtained. For each TAC we calculated estimates of the tracer DVR_L, DVR_r and BP_L and BP_r and eventually their coefficients of variation (COV). The analysis was performed for two tracers, since the outcome is dependent on the relative tracer accumulation in the target and reference regions, which varies for different tracers, as well as on tracer kinetics. Simulation studies by Meikle *et al* (2000) in fact showed that the BP of tracers with slower kinetics is more susceptible to a low statistical quality of the data compared to tracers with faster kinetics.

Since measured attenuation had been identified as a significant source of instrumentation-related inaccuracy for this scanner, the analysis was performed on rat and phantom data reconstructed with measured attenuation correction factors and attenuation correction factors obtained after appropriately segmenting the attenuation maps into pre-defined μ-values.

Given a certain injected dose, the number of acquired counts depends mostly on the scanner sensitivity (assuming, as mentioned earlier, that the count rates are well below the count rate capabilities of the scanner). The results presented here are thus valid for the specific scanner used, the Concorde microPET® R4 (Knoess *et al* 2003), which has an absolute sensitivity of approximately 2% and the specific image correction and reconstruction algorithms used. The methodological procedure presented in this paper is, however, not only directly applicable to any other scanner, but can also be used to compare various data quantification and reconstruction algorithms in terms of their impact on the variability of a final PET outcome measure.

Methods

Rat studies

Data from two MP and two DTBZ studies on the same rat were used to obtain the TACs which served as templates when forming TACs from the phantom study. In all cases rats were injected with 3.7 MBq/100 g of tracer with sufficiently high specific activity to satisfy the tracer principle requirement. Each study consisted of a 10 min transmission scan using a ^{68}Ge point source with single event acquisition mode, followed by 6 × 30 s, 2 × 60 s, 5 × 300 s, 2 × 450 and 2 × 480 s of emission data for a total of 60 min. Images were reconstructed with all corrections except for decay, using Fourier rebinning and FBP. For the data normalization procedure, a component-based normalization method was used, which has

been recently shown to provide an optimum image uniformity (Camborde *et al* 2004). Separate reconstructions were performed for segmented and measured attenuation correction. In the segmented attenuation correction method, an attenuation image is first reconstructed from measured data and pre-defined μ-values are assigned to specific regions after performance of threshold-based segmentation. For the purpose of this study, the striatal TAC was obtained from the average of six striatal 6.4 mm^2 regions of interest ROIs (placed on the left and right striatal images on three consecutive axial planes). The reference region template TAC was obtained from two 20 mm^2 ROIs placed on the cerebellar region (one on each contiguous axial plane) which is typically located approximately 11 axial planes (1.2 cm) posterior to the striatum. The ROIs were taken from a template which is commonly used in our centre. During our standard analysis of the rat data, a separate TAC is formed for each striatum by averaging the values of the ROIs on the three adjacent axial planes. The cerebellar TAC is obtained from an average of two 20 mm^2 ROI values placed on two adjacent axial planes. All studies were performed on a CTI-Concorde microPET® R4 (Knoess *et al* 2003), which has a spatial resolution of approximately $(1.8\ mm)^3$, with a slice separation of 1.2 mm.

Phantom studies—choice of phantom

The TACs used in the Logan and ratio analysis are obtained from PET data that are fully corrected except for the overall sensitivity calibration (conversion from count density to concentration), which is in this case not needed, since a tissue input method is used for further data analysis. Such corrections, for example attenuation and scatter corrections, alter the final image intensity values. The magnitude of these correction factors depends on the density and size of the object being scanned. It was thus important that the size and density of the phantom used in this study closely resembled the size and density of a rat. We found that a 2.5 cm diameter cylinder filled with an aqueous radioactivity concentration provided a good match. The accuracy of the match was verified by ensuring that the ratio between image intensity values of a ROI centrally placed on the scatter and attenuation corrected image and the same ROI placed on the uncorrected image was very similar for both for the phantom and the rat studies. We could thus assume that the same image intensity values observed in the scatter and attenuation corrected phantom and rat study would be representative of the same number of acquired counts/voxel and thus total acquired counts originating from the specific region of interest for the same scan duration. The 2.5 cm diameter cylinder will be hereafter referred to as 'rat phantom'.

Phantom studies—scans performed

The 'rat phantom' was filled with an aqueous solution containing 35.4 MBq of ^{11}C and scanned for 3 h, covering a count rate range from 268.6×10^3 counts s^{-1} to 0.67×10^3 counts s^{-1}. The cylinder was placed into the rat head holder and positioned asymmetrically in the axial direction to simulate as close as possible the rat scanning conditions, including contributions from radioactivity from outside the field of view (FOV): lengthwise, a 5.5 cm long section of the phantom was outside the FOV, while a 6.5 cm section was located inside the FOV. List mode acquired data were binned into 30 s intervals and reconstructed with all corrections except for decay using Fourier rebinning and FBP. As for the rat studies, data were reconstructed separately with measured and segmented attenuation correction.

Formation of phantom TACs

'Rat-phantom' data sets were extracted from the phantom study by selecting those frames where the measured concentration in the phantom study matched that in a selected rat TAC

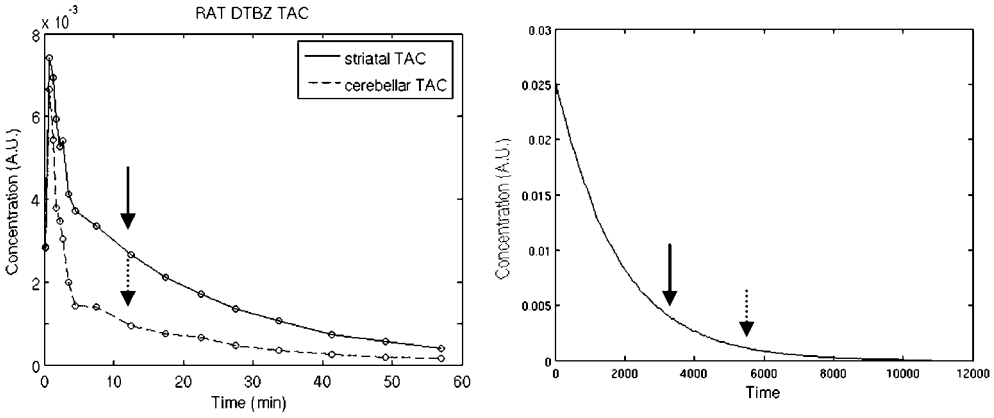

Figure 1. Example of matching the concentration of measured in a rat TAC (left) with selected frames of the phantom TAC (right) to form the rat phantom TAC curves. All curves are without decay correction. The arrows indicate which phantom time frame was chosen to represent the radioactivity of that particular point in the rat TAC. The solid line only connects the measured points (o). In the case of the phantom data (figure on the right) the points are so close together that the solid line effectively represents the individual points.

(figure 1). The average over all planes of the phantom study was used to define the appropriate 'rat-phantom' data sets so as to avoid possible inconsistencies due to potential local non-uniformities in the phantom image. In order to match for the frame duration of the rat studies and consequently the number of acquired counts originating from a specific region, the appropriate number of 30 s frames of the phantom data was added together (appropriately centred around the identified matching 30 s frame). The result was thus a unique 17 frame subset of the entire phantom data set for each rat TAC.

Once the appropriate dynamic sequence of phantom images was formed, ROIs of the same size as those used in the rat image analysis were placed on the phantom image. 66 striatal size (9 pixels) and 60 cerebellar size (28 pixels) ROIs were placed across several axial planes on each frame of the dynamic sequence. Since these ROIs were placed on images of a uniform phantom, the only difference between them was assumed to be of statistical nature with a possible contribution from instrumentation- or algorithm-introduced non-uniformities. Once the TACs were formed as described, the appropriate decay corrections relative to the rat data framing sequence (see Rat studies) were applied to replicate the TACs used in our implementation of the Logan analysis, which requires decay corrected data.

Image analysis and statistical analysis of results

The effect of measurement uncertainty was evaluated for four parameters BP_L, BP_r, DVR_L and DVR_r. Since these parameters are often calculated on TACs obtained as averages from single ROI TACs (see Rat studies), we investigated the variation of the parameter COV as a function of ROI averaging. We also compared the average BP values to investigate for the presence of a possible parameter bias as a function of ROI averaging. The parameters estimates were thus calculated for the TAC formed as described in table 1. Str3_Cer2 is the method that effectively corresponds to that used in the standard analysis of the rat data in our centre. The figure of merit used to describe the statistical accuracy of the data was the COV. An overall coefficient of variation (COV_o) was calculated for each method by estimating the mean and standard deviation of each parameter obtained with each striatal and cerebellar TAC combination.

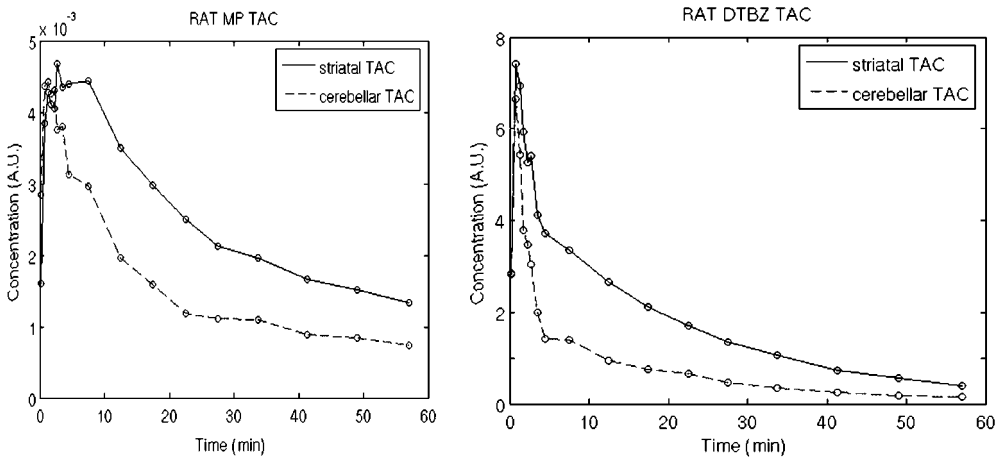

Figure 2. TACs from an MP and a DTBZ rat scan for the striatum and cerebellum. Here again the lines just connect the points (o).

Table 1. Number of ROIs contributing to the formation of the TACs used in the evaluation of the four parameters.

Method	Striatal TAC (number of TACs)	Cerebellar TAC (number of TACs)	Total number of estimates
Str_Cer_Ind	Individual ROI (66)	Individual ROI (60)	3960
Str_2	Average over 2 ROIs (33)	Individual (60)	1980
Str_3	Average over 3 ROIs (22)	Individual (60)	1320
Cer_2	Individual (66)	Average over 2 ROIs (30)	1980
Cer_3	Individual (66)	Average over 3 ROIs (20)	1320
Str2_Cer2	Average over 2 ROIs (33)	Average over 2 ROIs (30)	990
Str3_Cer2	Average over 3 ROIs (22)	Average over 2 ROIs (30)	660

In addition, we separated the contribution of the striatal and cerebellar data to the overall COV. To determine the COV due to the striatal TACs, the COV amongst the parameter values was calculated for each cerebellar TAC separately (that is keeping the same cerebellar TAC and varying the striatal TAC) and the resulting COV samples were averaged to produce the 'striatal COV' (COV_s). Likewise, to determine the COV due to the cerebellar TACs, the COV was calculated for each striatal TAC separately (that is keeping the striatal TAC the same and varying the cerebellar TAC) and the resulting COV samples were averaged to produce the 'cerebellar COV' (COV_c). This analysis was performed for each rat TAC template. The presented results are averages over data obtained from two rat templates for each tracer. In performing the analysis we ensured that the different number of TAC estimates (table 1) did not influence the statistical reliability of the COV determination.

Results

Rat and 'rat phantom' TACs

Figure 2 shows the decay corrected TACs obtained from one of the MP and one of the DTBZ rat scans illustrating the difference in their kinetic behaviour. A comparison between striatal and cerebellar TACs obtained from rat studies and the corresponding ones formed from the

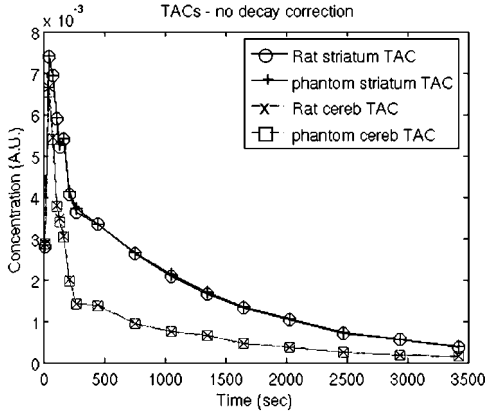

Figure 3. Comparison between the rat and 'rat phantom' TACs obtained from plane averages. The corresponding TACs are essentially overlaid. Here again the lines just connect the points.

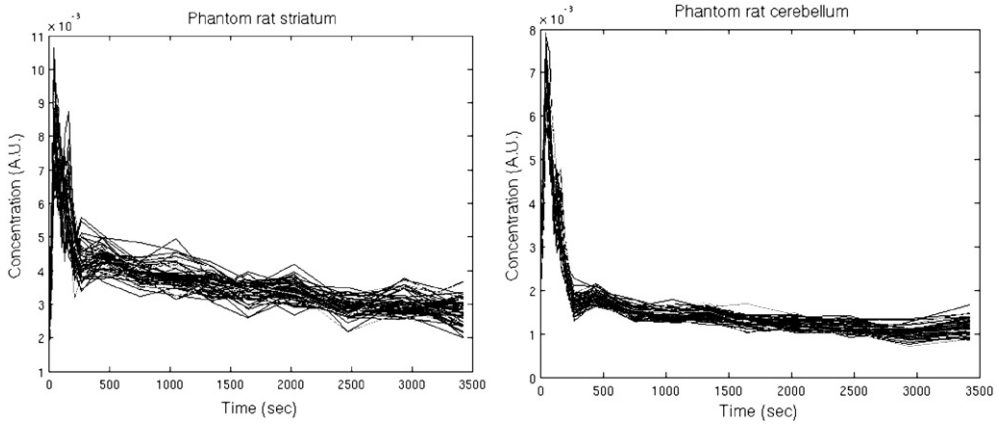

Figure 4. Example of TAC replicas obtained from the 'rat phantom' data for the striatum (left) and cerebellum (right).

rat phantom using plane averages (see methods) is shown in figure 3 emphasizing the good agreement between them. Finally, figure 4 shows an example of the replicas of the same TAC obtained from the 'rat phantom'data both for the cerebellar and the striatal TACs.

DVR and BP values

The DVR and BP values obtained with the different degree of ROI averaging were statistically indistinguishable (less than 2% difference between the values obtained with the different types of averaging), indicating that the averaging (or lack thereof) did not introduce any bias into the parameter estimate. It is well known that the Logan graphical approach suffers from a downward bias in the presence of noise (Slifstein and Laruelle 2000). However, it is also known that such bias decreases as a function of the numerical magnitude of the parameter being evaluated. In the tested cases the estimated DVR values were approximately 3 or smaller, a numerical range where the noise-induced bias becomes negligible. The DVR

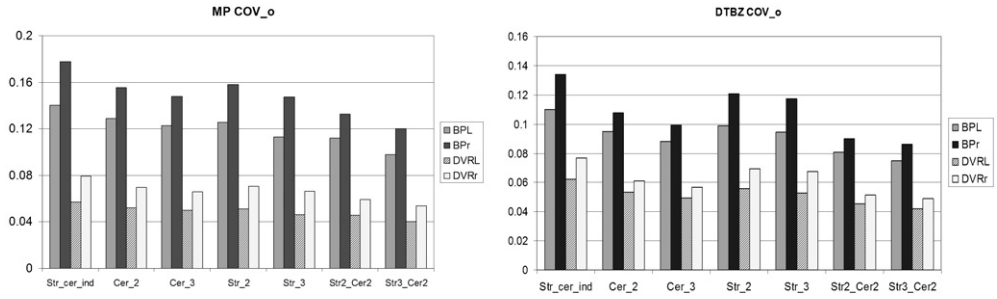

Figure 5. COV_o for the TAC configurations listed in table 1 for all four parameters (DVR and BP obtained with the Logan method and ratio methods—DVR_L, BP_L and DVR_r BP_r respectively) for MP (left) and DTBZ (right).

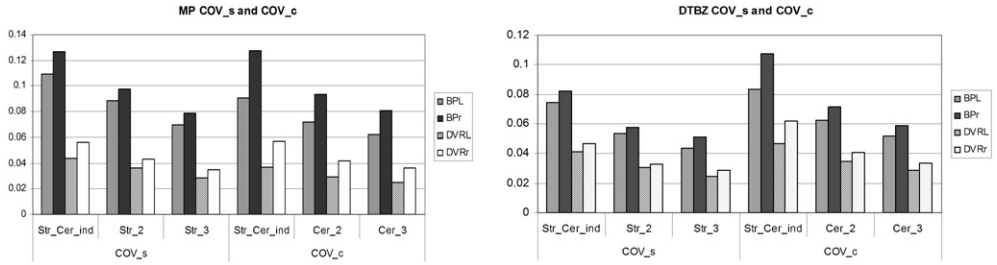

Figure 6. COV_s and COV_c for the TAC configurations listed in table 1 for all four parameters (DVR and BP obtained with the Logan method and ratio methods—DVR_L, BP_L and DVR_r BP_r respectively) for MP (left) and for DTBZ (right).

and BP obtained from data corrected with different attenuation corrected methods were also statistically indistinguishable, although, as will be pointed out in the coming discussion, those obtained from data corrected with measured attenuation had a much higher COV compared to those obtained with segmented attenuation correction.

COV analysis

The results of the COV analysis for the segmented attenuation corrected data are presented in figures 5 and 6, while a subset of equivalent results obtained for measured attenuation corrected data is shown in figure 7.

Discussion

The effect of several factors can be determined from the analysis of the data presented in figures 5–7 as discussed in the sections below.

Accuracy of attenuation correction effect

A comparison of the data in figures 5 and 7 clearly shows that the measured attenuation correction introduces significant non-uniformities into the images as investigated in detail in other studies (Camborde *et al* 2004). These non-uniformities manifest themselves both in

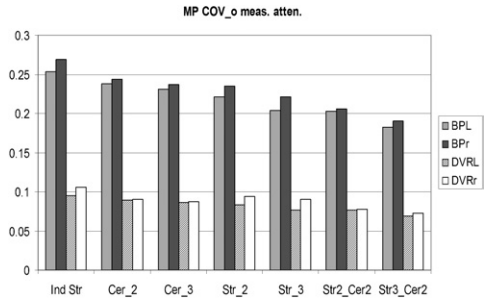

Figure 7. COV_o for the TAC configurations listed in table 1 for all four parameters (DVR and BP obtained with the Logan method and ratio methods—DVR_L, BP_L and DVR_r BP_r respectively) for measured attenuation. To be compared to data in figure 5.

terms of increased image noise compared to the case when segmented attenuation is used, and as a relatively systematic undercorrection in the radial and axial centre of the object image. These observations are explained by the fact that measured data are used directly (increase in noise) and by an inaccurate scatter correction of the transmission data (position-dependent attenuation undercorrection). In general, the BP COV approximately doubled compared to the case when segmented attenuation was used, without a significant change in the average BP or DVR values. Since the COV of the results obtained with the measured attenuation was so much higher the rest of the discussion will be focused onto the results obtained with segmented attenuation corrected data. Thus, all figures, except figure 7, show results from data processed with segmented attenuation correction.

Tracer effect

In agreement with the results of Meikle *et al* (2000), a greater COV was observed for MP, the tracer with slower kinetic. For the BP measures, for DTBZ the largest COV was 13.4%, while for the MP the largest COV was 17.8%. For the DVR measures, the corresponding values were 7.7% and 7.9% (figures 4 and 5). Both the MP and DTBZ scans were performed on the same rats, so as to minimize the influence of inter-subject variability on the tracer comparison.

Region of interest effect

As expected, larger COVs were obtained with no ROI averaging when calculating the TACs. In that case the COV values were those quoted in the section above (figure 5 and 6). In the case with the largest tested amount of averaging (striatal TAC averaged over three ROIs and cerebellar TAC averaged over two cerebellar ROIs—corresponding to the analysis method routinely used in our centre) the COV dropped to below approximately 8.6% for DTBZ and 12% for MP for the BP measures and below 5% and 5.4% respectively for the DVR measures. Due to the limited size of the rat brain, the inclusion of a larger number of ROIs in the determination of the TACs was considered unrealistic and was not performed.

When investigating the relative contribution of the striatal and cerebellar ROI to the overall COV, it was found that for MP the total COV has similar contribution from the variability of the striatal and the cerebellar region. In the DTBZ case the COVs of the cerebellar regions seem to contribute slightly more to the overall COV compared to COV_s. The differences can be likely attributed to different kinetic properties of the two tracers in the regions with and without specific binding. The overall approximate similarity of the two contributions can be

explained by the fact that the radiotracer concentration is higher in the striatum; however the ROI placed on the cerebellar region is larger, thus incurring less statistical noise.

Analysis method effect

Interestingly, the parameters determined with the Logan graphical approach appear more robust with respect to measurement uncertainties compared to those obtained with the ratio method, with total COVs that are generally 20% lower compared to those for the equivalent parameter estimates obtained with the ratio approach. In particular, the parameter estimates obtained with the ratio methods are much more sensitive to the variability of the cerebellar region. Data in figure 6 show not only that for the ratio method the COV due to the cerebellar region is higher, but also that the biggest contribution in noise reduction is obtained by estimating cerebellar TACs from averages of cerebellar ROIs.

The COV for the DVR estimates is clearly lower compared to that of the BP estimates, since the BP values are derived from the DVR values by subtracting 1. However, although DVR is directly measured, BP has a more relevant biological meaning, since it is more closely related to the tracer binding to the specific sites of interest. The BP COV estimates should thus be considered of primary importance when evaluating the effects of statistical and instrumentation-related inaccuracies on a biologically important outcome of reversible tracer PET studies.

The 'rat phantom' method

Although the 'rat phantom' method was designed to reproduce as accurately as possible the scanning conditions encountered in rat scanning, there are still some limitations in the complete generalization of the results from the phantom data to any individual rat scan. For example, in the ROI averaging, in the phantom case a homogeneous distribution of radioactivity is present throughout the ROI; this might not be the case when scanning rats, where the striatum is visible in three slices, but not necessarily with equal intensity (in the analysis of rat studies co-registration with anatomical information might possibly increase consistency in the delineation of the desired structures). Furthermore, we have performed the simulation assuming specific values for the DVR and BP determined from scans of two rats extracted from our general rat colony; in the general rat population there will be a range of DVR and thus BP values—so some numerical deviation from the results presented here may be expected. On the other hand, the rat phantom method has been designed in such a way as to allow the reproduction of any arbitrary TAC and it can thus be used to simulate any desired condition.

Conclusion

We developed a phantom and rat data based method that allows for the determination of the contribution of the measurement uncertainty to the variability of biological parameters. The method was applied to the data acquired with the microPET® R4 scanner. The analysis showed that measured attenuation correction in this particular scanner introduces noticeably more variability into the final results of the data analysis compared to segmented attenuation. A tracer and analysis method dependent variability was observed in the results, with COVs ranging from approximately 18% to 7.5% for BP estimates and 8% to 4% for the DVR measures. These values are quite comparable to those obtained in human reproducibility studies with the same tracers (Sossi *et al* 2000). It is thus reasonable to anticipate that the uncertainty introduced into the BP estimate by measurement errors will not be much greater in

rat studies using a microPET scanner compared to measurement currently performed in human scanners thus indicating that the microPET sensitivity is likely adequate for most dynamic ^{11}C studies.

Furthermore, the analysis has confirmed that methods used to extract DVR and BP are differently sensitive to the measurement uncertainties, with the graphical method proving more robust compared to the ratio method. The combination of averaging over as many ROIs as feasible and using a graphical approach for parameter determination together with a segmented attenuation correction method have been shown to produce fairly robust BP and DVR estimates at injected doses that to not violate the tracer principle. In addition to providing useful data in the studies presented here, the described method can be used to further explore the effect of data acquisition and processing on the variability of the final, biologically relevant parameters as well as comparing the sensitivity of various parameter extracting methods to statistical and instrumentation-related uncertainties.

Acknowledgments

The authors wish to thank Siobhan McCormick for assistance in data analysis and rat scanning, and Rick Kornelsen and Ivan Cepeda for assistance in rat scanning. This work has been supported by the National Science and Research Council (VS, AR), the Michael Smith Foundation for Health Research (VS), the Canadian Institutes for Health Research and a Triumf Life Science grant.

References

Camborde M L, Rahmim A, Newport D, Siegel S, Buckley K R, Vandervoort E, Ruth T J and Sossi V 2004 Effect of normalization method on image uniformity and binding potential estimates on microPET® *Proc. 2004 IEEE/MIC (Rome)*

Gunn R N, Lammertsma A A, Hume S P and Cunningham V J 1997 Parametric imaging of ligand-receptor binding in PET using a simplified reference region model *Neuroimage* **6** 279–87

Hume S P, Gunn R N and Jones T 1998 Pharmacological constraints associated with positron emission tomographic scanning of small laboratory animals *Eur. J. Nucl. Med.* **25** 173–6

Ito H, Hietala J, Blomqvist G, Halldin C and Farde L 1998 Comparison of the transient equilibrium and continuous infusion method for quantitative PET analysis of [11C]raclopride binding *J. Cereb. Blood Flow Metab.* **18** 941–50

Knoess C *et al* 2003 Performance evaluation of the microPET R4 PET scanner for rodents *Eur. J. Nucl. Med. Mol. Imaging* **30** 737–47

Lammertsma A A, Bench C J, Hume S P, Osman S, Gunn K, Brooks D J and Frackowiak R S 1996 Comparison of methods for analysis of clinical [11C]raclopride studies *J. Cereb. Blood Flow Metab.* **16** 42–52

Lammertsma A A and Hume S P 1996 Simplified reference tissue model for PET receptor studies *Neuroimage* **4** 153–8

Logan J, Fowler J S, Volkow N D, Wang G J, Ding Y S and Alexoff D L 1996 Distribution volume ratios without blood sampling from graphical analysis of PET data *J Cereb. Blood Flow Metab.* **16** 834–40

Logan J, Fowler J S, Volkow N D, Wolf A P, Dewey S L, Schlyer D J, MacGregor R R, Hitzemann R, Bendriem B and Gatley S J 1990 Graphical analysis of reversible radioligand binding from time-activity measurements applied to [N-11C-methyl]-(-)-cocaine PET studies in human subjects *J. Cereb. Blood Flow Metab.* **10** 740–7

Meikle S R, Eberl S, Fulton R R, Kassiou M and Fulham M J 2000 The influence of tomograph sensitivity on kinetic parameter estimation in positron emission tomography imaging studies of the rat brain *Nucl. Med. Biol.* **7** 617–25

Slifstein M and Laruelle M 2000 Effects of statistical noise on graphic analysis of PET neuroreceptor studies *J. Nucl. Med.* **41** 2083–8

Sossi V, Holden J E, Chan G, Krzywinski M, Stoessl A J and Ruth T J 2000 Analysis of four dopaminergic tracers kinetics using two different tissue input function methods *J. Cereb. Blood Flow Metab.* **20** 653–60